Article

Elastic Parameters of Paramagnetic Fe–20Cr–20Ni-Based Alloys: A First-Principles Study

Noura Al-Zoubi

Department of Applied Physics, Tafila Technical University, Tafila 66110, Jordan; noura@ttu.edu.jo

check for updates

Abstract: The single-crystal and polycrystalline elastic parameters of paramagnetic $Fe_{0.6-x}Cr_{0.2}Ni_{0.2}M_x$ (M = Al, Co, Cu, Mo, Nb, Ti, V, and W; $0 \leq x \leq 0.08$) alloys in the face-centered cubic (fcc) phase were derived by first-principles electronic structure calculations using the exact muffin-tin orbitals method. The disordered local magnetic moment approach was used to model the paramagnetic phase. The theoretical elastic parameters of the present Fe–Cr–Ni-based random alloys agree with the available experimental data. In general, we found that all alloying elements have a significant effect on the elastic properties of Fe–Cr–Ni alloy, and the most significant effect was found for Co. A correlation between the tetragonal shear elastic constant C' and the structural energy difference ΔE between fcc and bcc lattices was demonstrated. For all alloys, small changes in the Poisson's ratio were obtained. We investigated the brittle/ductile transitions formulated by the Pugh ratio. We demonstrate that Al, Cu, Mo, Nb, Ti, V, and W dopants enhance the ductility of the Fe–Cr–Ni system, while Co reduces it. The present theoretical data can be used as a starting point for modeling the mechanical properties of austenitic stainless steels at low temperatures.

Keywords: exact muffin-tin orbitals method; austenitic stainless steel; elastic constants; random alloys; density functional theory

1. Introduction

Austenitic stainless steels are paramagnetic alloys having the face-centered cubic (fcc) crystallographic structure. They are mainly composed of Fe, a minimum of 12 atomic percentage of chromium, a minimum of 6 atomic percentage of Ni, and low amounts of carbon and nitrogen. Austenitic stainless steels have excellent corrosion resistance and good mechanical properties such as ductility, strength, stiffness, and toughness [1]. Austenitic stainless steels have a wide range of applications, such as kitchen utensils, construction, equipment for the chemical industry and food processing, heat exchangers, etc. [2].

Single-crystal and polycrystalline elastic parameters are essential in determining the mechanical properties of the materials, such as hardness, fracture, ductility, and brittleness. These parameters measure the resistance of materials to external forces, and they determine the bulk modulus B, shear modulus G, Young's modulus E, and Poisson's ratio v. Alloying is important in tuning the fundamental properties of materials and in designing advanced engineering materials. Different alloying elements have specific effects on the materials. In austenitic stainless steels, the major alloying elements are chromium and nickel. Chromium gives the austenitic stainless steels corrosion resistance [3], while nickel is added to austenitic stainless steels to promote the austenite microstructure and to increase the ductility and toughness of steels. Other alloying elements determine the property profiles of certain grades of austenitic stainless steels. Many experimental studies have investigated the elastic properties of austenitic stainless steels [4–8]. In contrast to the experimental side, there are only a few theoretical studies of the elastic properties of austenitic stainless steels [9–11]. The principal purpose of this first-principles study is to fill this gap and to provide a comprehensive database

of the alloying effects on the elastic parameters of paramagnetic fcc Fe–20Cr–20Ni–xM. Specifically, we investigated the changes in the single-crystal and polycrystalline elastic constants caused by adding small concentrations of M (M = Al, Co, Cu, Mo, Nb, V, and W; $0 \leq x \leq 8$, where x is in atom %) that are soluble in the Fe–Cr–Ni system. We chose these alloying elements since they represent simple metal (Al), as well as nonmagnetic (Cu, Mo, Nb, V, and W) and magnetic (Co) transition metals. We excluded Cr and Ni from this study, since the effects of these alloying elements on the elastic properties of a paramagnetic fcc Fe–Cr–Ni system were discussed previously by Vitos et al. [11].

In the present work, all quaternary alloys were treated as substitutional disordered paramagnetic solid solutions with an ideal fcc structure. The paramagnetic phase was modeled using a disordered local moment scheme, which describes the systems well above the magnetic transition temperatures.

The rest of the paper includes two sections and conclusions. In Section 2, we describe the *ab initio* method, the elastic parameters, and the details of the numerical calculations. We present the results and the discussion in Section 3.

2. Methodology

2.1. Total Energy Calculations

The calculations in this work are based on density functional theory [12,13] and the Perdew-Burke-Ernzerhof (PBE) generalized gradient approximation [14] for the exchange correlation functional. The exact muffin-tin orbitals (EMTO) method [10,15–19] in combination with the scalar-relativistic scheme and soft-core approximation was used to solve the Kohn-Sham equations. The chemical and magnetic substitutional disorder was treated using coherent potential approximation (CPA) [20,21]. The total energy was computed using full charge density (FCD) approximation [22]. The paramagnetic state of the Fe–Cr–Ni–M alloys was simulated by the disordered local moments (DLM) model [23]. Within the DLM picture, a paramagnetic Fe–Cr–Ni–M quaternary alloy is described as an eight-component $(Fe^{\uparrow}Fe^{\downarrow})_{0.6-x}(Cr^{\uparrow}Cr^{\downarrow})_{0.2}(Ni^{\uparrow}Ni^{\downarrow})_{0.2}(M^{\uparrow}M^{\downarrow})_{x}$ alloy with equal amounts of spin up ($\uparrow$) and spin down ($\downarrow$) components. Using the DLM scheme, the impact of the loss of the magnetic moment above the Curie temperature on the total energy is properly taken into account, although our calculations were formally still performed at 0 K.

The equations of state and elastic parameters of the present Fe-based alloys and transition metal alloys were calculated using the EMTO method which was used in several former works [9,11,24–31].

2.2. Elastic Constants

The elastic properties of mono-crystalline materials are described by the elements C_{ij} of the elasticity tensor. There are three independent elastic constants for a cubic lattice C_{11}, C_{12}, and C_{44} and they are connected to the tetragonal shear elastic constant $C' = (C_{11} - C_{12})/2$ and bulk modulus $B = (C_{11} + 2C_{12})/3$. Dynamical (mechanical) stability requires that $C_{44} > 0$, $C' > 0$, and $B > 0$.

The cubic shear elastic constants C' and C_{44} were computed by keeping the volume constant during deformations of the conventional cubic cell. For the tetragonal shear modulus C', the following orthorhombic deformation was used:

$$\begin{pmatrix} 1+\delta_o & 0 & 0 \\ 0 & 1-\delta_o & 0 \\ 0 & 0 & \frac{1}{1-\delta_o^2} \end{pmatrix}.$$

This leads to the energy change

$$\Delta E(\delta_o) = 2VC'\delta_o^2 + O\left(\delta_o^4\right). \tag{1}$$

The C_{44} shear modulus was determined from the monoclinic distortion

$$
\begin{pmatrix}
1 & \delta_m & 0 \\
\delta_m & 1 & 0 \\
0 & 0 & \frac{1}{1-\delta_m^2}
\end{pmatrix}
$$

yielding

$$\Delta E(\delta_m) = 2VC_{44}\delta_m^2 + O\!\left(\delta_m^4\right) \tag{2}$$

In the above expressions, δ is the strain parameter.

Figure 1a,b represents an example of polynomial fit carried out for the above two equations (Equations (1) and (2)) which represent the constant volume (equilibrium volume) total energy change as functions of orthorhombic and monoclinic deformations, respectively. Panels (c) and (d) in Figure 1 show the standard errors in C' and C_{44}, respectively, of paramagnetic fcc Fe–Cr–Ni–Al alloys based on the polynomial fit.
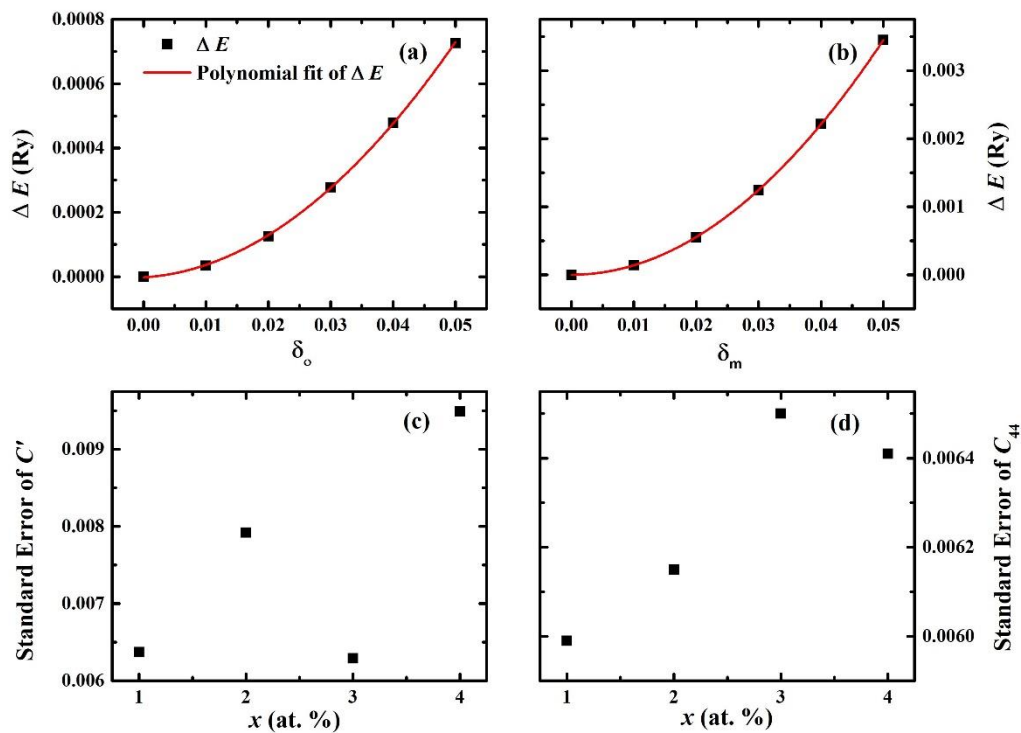

Figure 1. (**a**) Total energy change (Equation (1)) as a function of orthorhombic deformation δ_o of the fcc structure of a paramagnetic $Fe_{0.59}Cr_{0.2}Ni_{0.2}Al_{0.01}$ alloy. (**b**) Total energy change (Equation (2)) as a function of the monoclinic deformation δ_m of the fcc structure of a paramagnetic $Fe_{0.59}Cr_{0.2}Ni_{0.2}Al_{0.01}$ alloy. The red curves in (**a**) and (**b**) represent the polynomial fit of the total energy change. (**c**) The standard error in C' and (**d**) the standard error in C_{44} of $Fe_{0.6-x}Cr_{0.2}Ni_{0.2}Al_x(x = 0.01, 0.02, 0.03, 0.04)$ alloys as a function of x.

In polycrystalline materials, the mono-crystalline grains are misoriented. On a large scale, these materials can be considered as isotropic materials. The isotropic solids can be described by their bulk modulus B and shear modulus G. One can establish the *ab initio* polycrystalline elastic moduli by transforming single-crystal elastic constants C_{ij} to macroscopic quantities by suitable averaging methods based on statistical mechanics. For a cubic lattice, the polycrystalline bulk modulus is identical to the single-crystal bulk modulus. For the shear modulus, there are several different techniques for

averaging the single-crystal data. Here, we adopted the arithmetic Hill [32] average $G = (G_V + G_R)/2$, where the Voigt [33] and Reuss [34] limits are given in terms of single-crystal elastic constants, namely,

$$G_R = 5(C_{11} - C_{12})C_{44}/(4C_{44} + 3C_{11} - 3C_{12}) \tag{3}$$

$$G_V = (C_{11} - C_{12} + 3C_{44})/5 \tag{4}$$

The Young's modulus *E* and Poisson's ratio *ν* are related to *B* and *G* by the relations

$$E = 9BG/(3B + G) \tag{5}$$

$$\nu = (3B - 2G)/(6B + 2G) \tag{6}$$

In the present study, the single-crystal and polycrystalline elastic constants of the paramagnetic $Fe_{0.6-x}Cr_{0.2}Ni_{0.2}M_x$ (where M = Al, Co, Cu, Mo, Nb, Ti, V, and W; $0 \leq x \leq 0.08$) quaternary alloys were calculated for fcc lattices. The properties are presented and analyzed as a function of the atomic concentration *x*. Different atomic concentrations were used for each alloying element depending on their real solubility in austenitic $Fe_{0.6-x}Cr_{0.2}Ni_{0.2}M$ stainless steel.

2.3. Numerical Details

Green's function was computed for 16 complex energy points distributed exponentially on a semicircular contour. The *s*, *p*, *d*, and *f* orbitals were included in the EMTO basis set and $l^h_{\max} = 8$ was used in the one-center expansion of the full charge density [10]. The calculations are presented for paramagnetic fcc alloys. The total energy was evaluated by the shape function technique. The screened impurity model [35] with a screening parameter of 0.6 was used to describe the electrostatic correction to the single-site coherent potential approximation. For all components of the alloy, we chose the radii of the potential spheres to be equal to the corresponding average radii of the atomic spheres.

The bulk moduli of $Fe_{0.6-x}Cr_{0.2}Ni_{0.2}M_x$ alloys at their equilibrium volumes estimated from Equation (7) were derived from an exponential Morse-type function [36] installed with the ab initio total energies calculated for seven different atomic volumes; these volumes were expressed in terms of Wigner-Seitz radii *w* in the range 2.55 Bohr $\leq w \leq$ 2.70 Bohr in steps of 0.025 Bohr, including the equilibrium Wigner-Seitz radius. We considered six orthorhombic and monoclinic distortions with δ = 0, 0.01, 0.02, 0.03, 0.04, and 0.05. We used 1331–1694 uniformly distributed *k*-points in the irreducible wedge of the monoclinic and orthorhombic Brillouin zones to get the accuracy needed for the calculation of elastic constants.

3. Results and Discussions

3.1. Assessing the Accuracy of the Paramagnetic fcc Fe–20Cr–20Ni Alloy

We started our study by assessing the accuracy of our method with available experimental methods. In Table 1, we compare our results of single-crystal and polycrystalline elastic constants for the $Fe_{0.6}Cr_{0.2}Ni_{0.2}$ alloy with the experimental results [8] for the $Fe_{0.62}Cr_{0.19}Ni_{0.19}$ alloy, which is the closest alloy that we found to compare with. All theoretical elastic parameters for the $Fe_{0.6}Cr_{0.2}Ni_{0.2}$ alloy were calculated at the lattice parameter a = 3.58 Å estimated from Equation (7), and the experimental elastic parameters for the $Fe_{0.62}Cr_{0.19}Ni_{0.19}$ alloy were calculated at their experimental volume a = 3.55 Å [8]. We obtained agreement between our results and the experimental results, and we found that the theoretical C_{11}, C_{12}, and *C'* values were smaller than the experimental values by 13.2%, 6.8%, and 25.1%, respectively. The calculated C_{44} was larger than the experimental value by 3.9%. We ascribe the worse agreement in the case of *C'* to the different experimental volumes used in both methods and to the small differences in concentrations of alloying elements in both systems. The theoretical polycrystalline elastic constants *B*, *E*, and *G* were smaller than the experimental values by 9.4%, 9.2%, and 9.2%, respectively. On the other hand, the *B/G* ratio and Poisson's ratio *ν* were

accurately reproduced by our method. Compared to the experiment data, they deviated by 0.27% and 0.17%, respectively.

Table 1. Theoretical (exact muffin-tin orbitals, EMTO) and experimental (Exp) [8] elastic constants (in GPa) for paramagnetic fcc Fe–Cr–Ni alloys. *B/G* and ν are dimensionless. In the last row, we present the percentage error between the experimental and theoretical elastic constants.

System	C_{11}	C_{12}	C'	C_{44}	B	E	G	B/G	ν
$Fe_{0.6}Cr_{0.2}Ni_{0.2}$ (EMTO)	177	124	26.6	131	142	181	70.1	2.03	0.288
$Fe_{0.62}Cr_{0.19}Ni_{0.19}$ (Exp)	204	133	35.5	126	157	199	77.2	2.03	0.289
Percentage error (%)	13.2	6.8	25.1	3.9	9.4	9.2	9.2	0.27	0.17

Having demonstrated the accuracy of our method, we expanded our study to Fe–Cr–Ni systems containing different concentrations of Al, Co, Cu, Mo, Nb, Ti, V, and W and investigated the alloying effects on the single and polycrystalline elastic constants of the Fe–Cr–Ni system.

3.2. Single-Crystal Elastic Constants

Dyson and Holmes [37] applied X-ray methods to an austenite standard of known lattice parameter, and they observed predominantly linear variation in the lattice parameter with variation in the amount of alloying element in the austenite steel. They performed linear multiple regression analysis. The variation in the lattice parameter of austenite with respect to the atom % values of alloying elements using regression analysis was

$$a\ (\text{Å}) = 3.577 + 0.0065\text{C} + 0.0010\text{Mn} - 0.0002\text{Ni} + 0.0006\text{Cr} + 0.0056\text{N} + 0.0028\text{Al} - 0.004\text{Co} + 0.0014\text{Cu} + 0.0053\text{Mo} + 0.0079\text{Nb} + 0.0032\text{Ti} + 0.0017\text{V} + 0.0057\text{W}. \tag{7}$$

According to Equation (7), Al, Cu, Mo, Nb, Ti, V, and W dopants enlarge the lattice parameter of austenite steel, while Co deceases it. In Figure 2, using Equation (7), we display the changes in the equilibrium lattice parameter for paramagnetic fcc $Fe_{0.6-x}Cr_{0.2}Ni_{0.2}M_x$ (M = Al, Co, Cu, Mo, Nb, Ti, V, and W; $0 \le x \le 0.08$) quaternary alloys relative to the paramagnetic fcc $Fe_{0.6}Cr_{0.2}Ni_{0.2}$ ternary alloy as a function of the atomic concentrations x of alloying elements. The numerical values of the lattice parameters, based on Equation (7), of the paramagnetic fcc $Fe_{0.6-x}Cr_{0.2}Ni_{0.2}$-based alloys are listed in Tables 2 and 3.
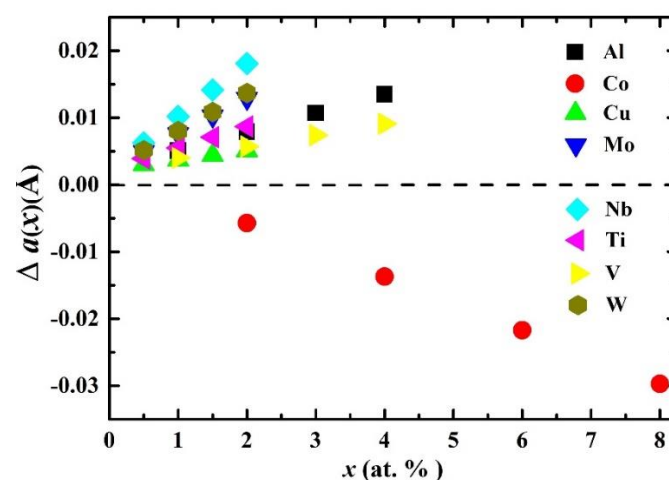

Figure 2. Changes in the equilibrium lattice parameters ($a(x)$), based on Equation (7), of paramagnetic fcc $Fe_{0.6-x}Cr_{0.2}Ni_{0.2}M_x$ (where M = Al, Co, Cu, Mo, Nb, Ti, V, and W; $0 \le x \le 0.08$) quaternary alloys relative to the paramagnetic fcc $Fe_{0.6}Cr_{0.2}Ni_{0.2}$ ternary alloy as a function of atomic concentration x.

Table 2. Theoretical (EMTO) single-crystal elastic constants (in GPa) for paramagnetic fcc Fe–20Cr–20Ni–x%M (M = Al, Co, Cu, Mo, Nb, Ti, V, and W; $0 \leq x \leq 8$, where x is in atom %) alloys calculated at their lattice parameter a_{exp} (in Å) estimated from Equation (7).

System	a_{exp}	C_{11}	C_{12}	C'	C_{44}
Fe–20Cr–20Ni	3.583	177	124	26.6	131
Fe–20Cr–20Ni–1.0Al	3.588	176	125	25.4	130
Fe–20Cr–20Ni–2.0Al	3.591	176	127	24.6	129
Fe–20Cr–20Ni–3.0Al	3.593	176	129	23.2	129
Fe–20Cr–20Ni–4.0Al	3.596	177	131	22.8	128
Fe–20Cr–20Ni–2.0Co	3.577	183	125	28.7	136
Fe–20Cr–20Ni–4.0Co	3.569	190	128	30.8	140
Fe–20Cr–20Ni–6.0Co	3.561	197	131	32.7	145
Fe–20Cr–20Ni–8.0Co	3.553	204	134	34.9	149
Fe–20Cr–20Ni–0.5Cu	3.586	177	124	26.5	130
Fe–20Cr–20Ni–1.0Cu	3.586	177	125	26.1	130
Fe–20Cr–20Ni–1.5Cu	3.587	178	126	25.9	129
Fe–20Cr–20Ni–2.0Cu	3.588	178	127	25.6	129
Fe–20Cr–20Ni–0.5Mo	3.588	181	128	26.3	130
Fe–20Cr–20Ni–1.0Mo	3.590	181	129	25.9	130
Fe–20Cr–20Ni–1.5Mo	3.593	181	130	25.4	130
Fe–20Cr–20Ni–2.0Mo	3.596	180	130	25.0	130
Fe–20Cr–20Ni–0.5Nb	3.589	176	124	25.9	130
Fe–20Cr–20Ni–1.0Nb	3.593	176	126	24.8	129
Fe–20Cr–20Ni–1.5Nb	3.597	175	127	24.0	128
Fe–20Cr–20Ni–2.0Nb	3.601	176	129	23.2	127
Fe–20Cr–20Ni–0.5Ti	3.587	177	126	25.8	130
Fe–20Cr–20Ni–1.0Ti	3.588	176	126	24.9	129
Fe–20Cr–20Ni–1.5Ti	3.590	177	128	24.2	128
Fe–20Cr–20Ni–2.0Ti	3.591	176	129	23.4	128
Fe–20Cr–20Ni–1.0V	3.587	176	124	25.8	130
Fe–20Cr–20Ni–2.0V	3.588	177	127	24.8	129
Fe–20Cr–20Ni–3.0V	3.590	177	128	24.0	128
Fe–20Cr–20Ni–4.0V	3.592	177	130	23.5	127
Fe–20Cr–20Ni–0.5W	3.588	179	126	26.3	131
Fe–20Cr–20Ni–1.0W	3.591	181	129	26.0	131
Fe–20Cr–20Ni–1.5W	3.594	182	131	25.5	131
Fe–20Cr–20Ni–2.0W	3.596	184	134	25.0	131

Table 3. Theoretical (EMTO) polycrystalline elastic constants *B*, *G*, and *E* (in GPa); Poisson's ratio *v*; and *B*/*G* ratio for paramagnetic fcc Fe–20Cr–20Ni–*x*%M (M = Al, Co, Cu, Mo, Nb, Ti, V, and W; $0 \leq x \leq 8$, where *x* is in atom %) calculated at their experimental lattice parameter $a_{\exp}$ [37] (in Å).

System	$a_{\exp}$	*B*	*G*	*B*/*G*	*E*	*v*
Fe–20Cr–20Ni	3.583	142	70.1	2.03	181	0.288
Fe–20Cr–20Ni–1.0Al	3.588	142	68.6	2.06	177	0.292
Fe–20Cr–20Ni–2.0Al	3.591	143	67.6	2.12	175	0.296
Fe–20Cr–20Ni–3.0Al	3.593	145	66.0	2.19	172	0.302
Fe–20Cr–20Ni–4.0Al	3.596	146	65.4	2.24	171	0.305
Fe–20Cr–20Ni–2.0Co	3.577	145	73.7	1.96	189	0.282
Fe–20Cr–20Ni–4.0Co	3.569	149	77.1	1.93	197	0.279
Fe–20Cr–20Ni–6.0Co	3.561	153	80.5	1.90	206	0.276
Fe–20Cr–20Ni–8.0Co	3.553	157	84.1	1.87	214	0.273
Fe–20Cr–20Ni–0.5Cu	3.586	141	69.8	2.03	180	0.288
Fe–20Cr–20Ni–1.0Cu	3.586	142	69.3	2.05	179	0.290
Fe–20Cr–20Ni–1.5Cu	3.587	143	68.9	2.07	178	0.292
Fe–20Cr–20Ni–2.0Cu	3.588	144	68.5	2.10	177	0.295
Fe–20Cr–20Ni–0.5Mo	3.588	146	69.6	2.10	180	0.294
Fe–20Cr–20Ni–1.0Mo	3.590	147	69.2	2.12	180	0.296
Fe–20Cr–20Ni–1.5Mo	3.593	147	68.6	2.14	178	0.298
Fe–20Cr–20Ni–2.0Mo	3.596	147	68.2	2.15	177	0.299
Fe–20Cr–20Ni–0.5Nb	3.589	141	69.0	2.04	178	0.290
Fe–20Cr–20Ni–1.0Nb	3.593	143	67.7	2.10	175	0.295
Fe–20Cr–20Ni–1.5Nb	3.597	143	66.5	2.16	173	0.299
Fe–20Cr–20Ni–2.0Nb	3.601	145	65.4	2.22	171	0.304
Fe–20Cr–20Ni–0.5Ti	3.587	143	69.1	2.07	178	0.292
Fe–20Cr–20Ni–1.0Ti	3.588	142	68.0	2.09	176	0.294
Fe–20Cr–20Ni–1.5Ti	3.590	144	66.9	2.16	174	0.299
Fe–20Cr–20Ni–2.0Ti	3.591	145	65.9	2.20	172	0.303
Fe–20Cr–20Ni–1.0V	3.587	142	69.0	2.05	178	0.290
Fe–20Cr–20Ni–2.0V	3.588	144	67.8	2.12	176	0.297
Fe–20Cr–20Ni–3.0V	3.590	145	66.6	2.18	173	0.301
Fe–20Cr–20Ni–4.0V	3.592	146	65.8	2.22	172	0.304
Fe–20Cr–20Ni–0.5W	3.588	144	69.7	2.06	180	0.291
Fe–20Cr–20Ni–1.0W	3.591	146	69.6	2.10	180	0.295
Fe–20Cr–20Ni–1.5W	3.594	148	69.1	2.15	179	0.298
Fe–20Cr–20Ni–2.0W	3.596	151	68.7	2.20	179	0.302

Figure 3 represents the theoretical changes in single-crystal elastic constants (i.e., $\Delta C_{ij}(x) = C_{ij}(\text{Fe}_{0.6-x}\text{Cr}_{0.2}\text{Ni}_{0.2}\text{M}_x) - C_{ij}(\text{Fe}_{0.6}\text{Cr}_{0.2}\text{Ni}_{0.2})$) of paramagnetic fcc $\text{Fe}_{0.6-x}\text{Cr}_{0.2}\text{Ni}_{0.2}\text{M}_x$ (M = Al, Co, Cu, Mo, Nb, Ti, V, and W; $0 \leq x \leq 0.08$) random alloys relative to the paramagnetic fcc $\text{Fe}_{0.6}\text{Cr}_{0.2}\text{Ni}_{0.2}$ random alloy. In Table 2, we list the numerical values for C_{11}, C_{12}, C', and C_{44} of paramagnetic fcc $\text{Fe}_{0.6-x}\text{Cr}_{0.2}\text{Ni}_{0.2}$-based alloys calculated at their corresponding equilibrium lattice parameter $a_{\exp}$.
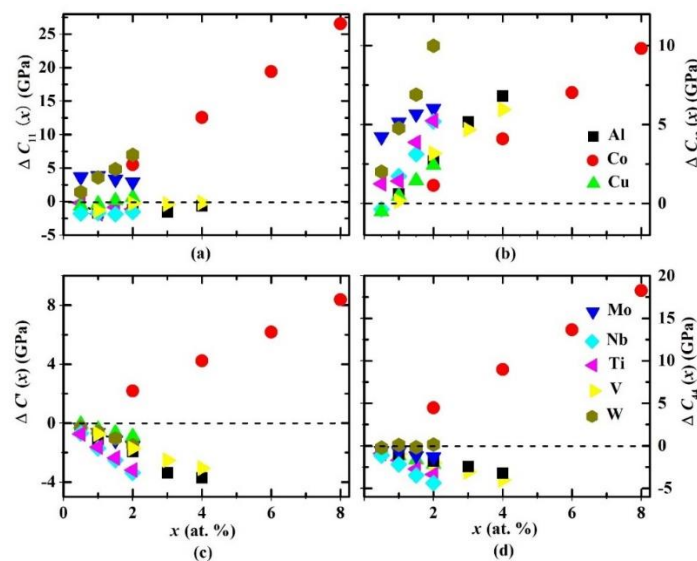
Figure 3. Theoretical changes in single-crystal elastic constants (**a**) $\Delta C_{11}(x)$, (**b**) $\Delta C_{12}(x)$, (**c**) $\Delta C'(x)$, and (**d**) $\Delta C_{44}(x)$ of paramagnetic fcc $Fe_{0.6-x}Cr_{0.2}Ni_{0.2}M_x$ (M = Al, Co, Cu, Mo, Nb, Ti, V, and W; $0 \leq x \leq 0.08$) quaternary alloys relative to the paramagnetic fcc $Fe_{0.6}Cr_{0.2}Ni_{0.2}$ ternary alloy as a function of atomic concentration x.

Investigating Figure 3 and Table 2, we observe that when adding 2.0 (0.5), 4.0 (1.0), 6.0 (1.5), and 8.0 (2.0) atom % of Co (W) to the paramagnetic fcc Fe–Cr–Ni alloy, the theoretical C_{11} increases by 5.5 (1.5), 12.6 (3.6), 19.4 (4.9), and 53.6 (7.0) GPa, respectively. Aluminum, copper, niobium, titanium, and vanadium were found to have negligible effects on the C_{11} value of the paramagnetic fcc Fe–Cr–Ni alloy. It is interesting to note that when substituting 0.5 atom % of Mo for Fe in the $Fe_{0.6}Cr_{0.2}Ni_{0.2}$ alloy, the C_{11} increases by 3.7 GPa, but further substitution of Mo (1.0, 1.5, and 2.0 atom %) for Fe has no effect on the C_{11} of the $Fe_{0.6}Cr_{0.2}Ni_{0.2}$ alloy.

The calculated C_{12} of the fcc Fe–Cr–Ni alloy increased with all alloying elements considered. Namely, the addition of 1.0, 2.0, 3.0, and 4.0 atom % of Al (V) to the $Fe_{0.6}Cr_{0.2}Ni_{0.2}$ alloy enhanced the C_{12} value by 0.6 (0.2), 2.7 (3.2), 5.2 (4.7), and 6.8 (6) GPa, respectively. Cobalt and tungsten had pronounced effects on the C_{12} value: adding 2.0 (0.5), 4.0 (1.0), 6.0 (1.5), and 8.0 (2.0) atom % of Co (W) to $Fe_{0.6}Cr_{0.2}Ni_{0.2}$ alloy yielded ΔC_{12} = 1.2 (2), 4.1 (4.8), 7 (6.9), and 9.8 (10) GPa. Substituting 0.5 atom % to 2.0 atom % of Cu, Mo, Nb, and Ti for Fe in the $Fe_{0.6}Cr_{0.2}Ni_{0.2}$ alloy increased C_{12} from ~1.2 GPa to ~4.4 GPa.

We then investigated the alloying effects on the shear elastic constant C_{44} of the $Fe_{0.6}Cr_{0.2}Ni_{0.2}$ alloy, and we found that Co is the only alloying element that enhanced C_{44}. Adding 2.0, 4.0, 6.0, and 8.0 atom % of Co to the $Fe_{0.6}Cr_{0.2}Ni_{0.2}$ alloy increased the C_{44} value by 4.5, 9.0, 13.7, and 18.3 GPa, respectively. Negative alloying effects on C_{44} of the fcc Fe–Cr–Ni alloy occurred for Al, Cu, Mo, Nb, Ti, and V. Substituting 1.0, 2.0, 3.0, and 4.0 atom % of Al (V) for Fe in the $Fe_{0.6}Cr_{0.2}Ni_{0.2}$ alloy reduced the C_{44} value by 1.0 (1.0), 1.8 (2.0), 2.5 (3.0), and 3.2 (4.0) GPa, respectively. On the other hand, adding 0.5 atom % to 2 atom % of Cu, Mo, Nb, and Ti changed ΔC_{44} from approximately −0.6 GPa to −3.4 GPa. Tungsten was found to have a negligible effect on C_{44}.

The tetragonal shear elastic constant C' is often used to describe the stability of cubic solids. Positive (negative) values of C' indicate a stable (unstable) structure. Investigating Figure 3, we observed that Co addition increased the C' value of paramagnetic fcc Fe–Cr–Ni alloy, while Al, Cu, Mo, Nb, Ti, V, and W additions decreased it. Adding 2.0, 4.0, 6.0, and 8.0 atom % of Co to $Fe_{0.6}Cr_{0.2}Ni_{0.2}$ enhanced C' by 2.1, 3.5, 6.1, and 8.3 GPa, while substituting 1.0, 2.0, 3.0, and 4.0 atom % of Al (V) for Fe in the $Fe_{0.6}Cr_{0.2}Ni_{0.2}$ alloy reduced the C' value by 1.2 (0.8), 2 (1.8), 3.4 (2.6), and 3.8 (3.1) GPa. The effects of the other alloying elements were similar to those of Al and V. Adding 0.5 atom % to 2 atom % of Cu, Mo, Nb, Ti, or W to the Fe–Cr–Ni alloy changed the $\Delta C'$ from approximately −0.1 GPa to approximately

−3.4 GPa, respectively. According to our calculations of C', we may conclude that the paramagnetic fcc Fe–Cr–Ni alloy becomes dynamically more stable with Co addition and less stable with Al, Cu, Nb, Mo, Ti, V, and W dopants.

The tetragonal shear elastic constant C' is connected to the structural energy difference ΔE (i.e., $\Delta E = E_{bcc} - E_{fcc}$) between the bcc and fcc lattices. The values of C' can be obtained from the curvature around the energy minimum along a constant-volume Bain path. In fact, the Bain path [38] is a martensitic path that connects the fcc and bcc lattices which can be described as a body-centered tetragonal (bct) structure; when the c/a ratio of the bct structure is 1, the structure is bcc, while when the c/a ratio reaches $\sqrt{2}$, the structure is called an fcc structure. We can understand the trends of the C' elastic constants by understanding the trends of ΔE. In Figure 4, we plot the C' of fcc (solid symbols) and bcc (open symbols) lattices of paramagnetic Fe–Cr–Ni-based alloys and ΔE (i.e., $\Delta E = E_{bcc} - E_{fcc}$).
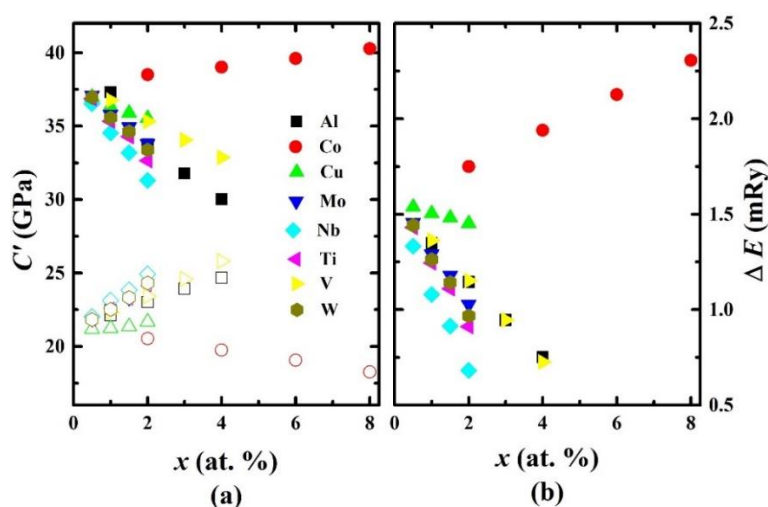

Figure 4. (**a**) Calculated fcc (solid symbols) and bcc (open symbols) tetragonal shear constant C′ values and (**b**) the calculated total energy difference ΔE ($\Delta E = E_{bcc} - E_{fcc}$) between the bcc and fcc structures of paramagnetic $Fe_{0.6-x}Cr_{0.2}Ni_{0.2}M_x$ (M = Al, Co, Cu, Mo, Nb, Ti, V, and W; $0 \leq x \leq 0.08$) quaternary alloys as a function of atomic concentration x.

Lacking experimental volume data for the paramagnetic bcc $Fe_{0.6-x}Cr_{0.2}Ni_{0.2}M_x$ (M = Al, Co, Cu, Mo, Nb, Ti, V, and W; $0 \leq x \leq 0.08$) random alloys, the C'_{fcc} and C'_{bcc} values and the total energies E_{bcc} and E_{fcc} in Figure 4 were calculated at their theoretical equilibrium volumes.

Investigating Figure 4a, we find that the C' values of all fcc paramagnetic Fe–Cr–Ni–M alloys are larger than those of the bcc lattices, which means that for all alloys considered, the fcc structure is more stable than the bcc structure. On the other hand, alloying has an impact on increasing or decreasing the fcc and bcc tetragonal elastic constants. We observe that the C'_{fcc} (C'_{bcc}) value of the Fe–Cr–Ni system increases (decreases) by addition of Co, while other alloying elements (Al, Cu, Mo, Nb, Ti, V, and W) reduce (enhance) the C'_{fcc} (C'_{bcc}) value of the Fe–Cr–Ni system. The structural energy difference ΔE (Figure 4b) has a similar (opposite) trend to that of C'_{fcc} (C'_{bcc}), with larger (smaller) values of ΔE corresponding to larger (smaller) values of C'_{fcc} (C'_{bcc}) of the Fe–Cr–Ni system. The scaling between C'_{fcc} (C'_{bcc}) and ΔE for Fe–Cr–Ni-based alloys holds. Our observations on the correlation between C' and ΔE are in line with those obtained by [39–44].

In summary, according to our calculations, the most significant effect on the C_{11}, C_{12}, C_{44}, and C' values of paramagnetic fcc Fe–Cr–Ni alloy was found for Co. The correlation between C' and the structural energy difference ΔE between the bcc and fcc lattices of the paramagnetic Fe–Cr–Ni system holds.

3.3. Polycrystalline Elastic Constants
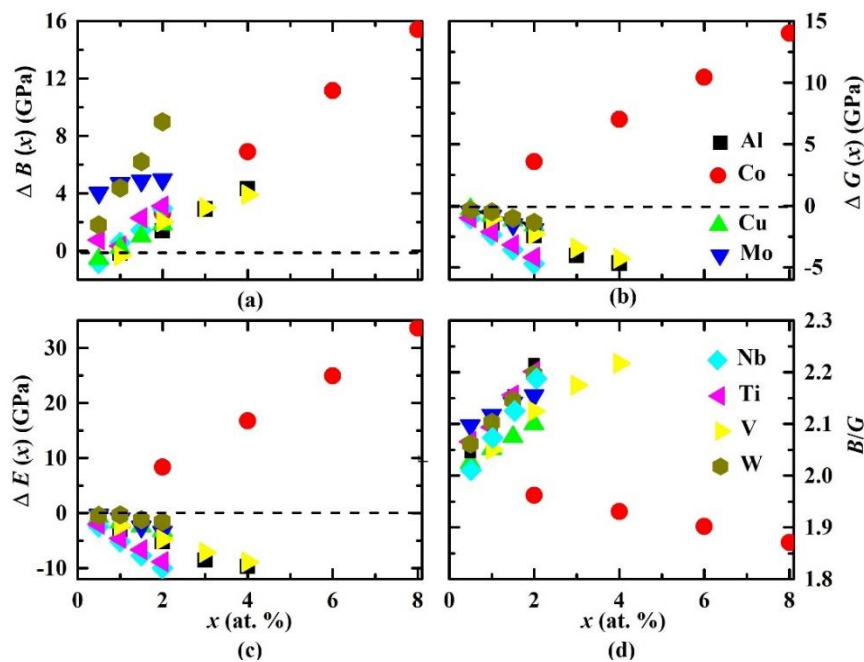
Theoretical changes in the polycrystalline elastic constants ($\Delta B(x)$, $\Delta G(x)$, $\Delta E(x)$) of paramagnetic fcc $Fe_{0.6-x}Cr_{0.2}Ni_{0.2}M_x$ (M = Al, Co, Cu, Mo, Nb, Ti, V, and W; $0 \leq x \leq 0.08$, where x is in atom %) random alloys relative to the paramagnetic fcc $Fe_{0.6}Cr_{0.2}Ni_{0.2}$ random alloy and B/G ratio are plotted in Figure 5. The numerical values of the polycrystalline elastic constants ($B(x)$, $G(x)$, $E(x)$), $B/G(x)$ ratio, and Poisson ratio $\nu(x)$ for paramagnetic fcc Fe–Cr–Ni-based alloys calculated at their experimental lattice parameters a_{exp} are listed in Table 3.

Figure 5. Theoretical changes in polycrystalline elastic constants (**a**) $\Delta B(x)$, (**b**) $\Delta G(x)$, and (**c**) $\Delta E(x)$ of paramagnetic fcc $Fe_{0.6-x}Cr_{0.2}Ni_{0.2}M_x$ (M = Al, Co, Cu, Mo, Nb, Ti, V, and W; $0 \leq x \leq 0.08$) quaternary alloys relative to those of the paramagnetic fcc $Fe_{0.6}Cr_{0.2}Ni_{0.2}$ ternary alloy, and (**d**) the B/G ratio as a function of atomic concentration x.

In Figure 5, we observe that all alloying elements enhanced the bulk modulus of the Fe–Cr–Ni system. The greatest alloying effect was found for Co, which increased the $B(x)$ of the Fe–Cr–Ni alloy to 3.6, 6.9, 11.2, and 15.4 GPa when adding 2.0, 4.0, 6.0, and 8.0 atom %. Aluminum and vanadium had an almost similar effect on the bulk modulus of the Fe–Cr–Ni system. Substituting 1.0, 2.0, 3.0, and 4.0 atom % of Al (V) for Fe in the $Fe_{0.6}Cr_{0.2}Ni_{0.2}$ alloy enhanced the bulk modulus by −0.2 (−0.3), 1.4 (2.0), 2.9 (3.0), and 4.3 (3.9) GPa, respectively. Tungsten had a significant effect on the bulk modulus. Namely, adding 0.5, 1.0, 1.5, and 2 atom % of W to the Fe–Cr–Ni alloy enhanced the bulk modulus by 1.8, 4.4, 6.2, and 9 GPa, respectively. Other alloying elements (Cu, Mo, Nb, Ti) enhanced the bulk modulus by small amounts ranging from approximately −0.8 GPa to approximately 5.0 GPa depending on the alloying elements' atomic concentrations. We attribute the increase of the bulk modulus when adding transition metals (Co, Cu, Mo, Nb, Ti, V, W) to the Fe–Cr–Ni alloy to the cohesion in *d* metals using the Friedel model [45,46], and also to the bond increase when going from 3*d* (Co, Cu, Ti, V) to 4*d* (Mo, Nb) and 5*d* (W) metals [47].

From Figure 5 and Table 3, we see that $\Delta G(x)$ and $\Delta E(x)$ have similar behavior. The variation of the shear modulus $G(x)$ and Young's modulus $E(x)$ increased when adding Co to the Fe–Cr–Ni alloy: adding 2.0–8.0 atom % of Co raised the G value (E value) of the Fe–Cr–Ni alloy by 3.6 (8.4) to 14.0 (33.6) GPa. On the other hand, Al, Cu, Mo, Nb, Ti, V, and W dopants reduced the $G(x)$ and $E(x)$ of the Fe–Cr–Ni alloy. The largest effect on $G(x)$ and $E(x)$ of Fe–Cr–Ni–M was produced by Co.

Investigating Figures 3 and 5, we note that the trends of $\Delta C'(x)$, $\Delta C_{44}(x)$, $\Delta G(x)$, and $\Delta E(x)$ are similar but are opposite to that of $\Delta a(x)$ from Figure 2. These trends can be explained using the following assumption based on the volume effect: Since Co addition decreases the average volume per atom in Fe–Cr–Ni (see Figure 2), it is also increasing the average bond strength and, therefore, the ability of the alloy to resist shear, while additions of Al, Cu, Nb, Mo, Ti, V, and W have the opposite effect. The addition of Al, Cu, Nb, Mo, Ti, V, or W to the fcc Fe–Cr–Ni alloy enlarges the lattice parameter and thus weakens the average bond strength between atoms; therefore, the ability of the alloy to resist shear decreases.

The ductile/brittle behavior of structural materials is important to their performance. Pugh [48] suggested a criterion that tests the ductility and brittleness of materials based on their bulk and shear moduli values: a material that has a B/G ratio less than 1.75 is in the brittle regime; otherwise, it is in the ductile regime. From Figure 5 and Table 3, we observed that the paramagnetic fcc $Fe_{0.6}Cr_{0.2}Ni_{0.2}$ alloy is in the ductile regime with B/G = 2.0253. Our calculations show that Al, Cu, Mo, Nb, Ti, V, or W addition to the paramagnetic fcc Fe–Cr–Ni system enhances B/G and increases the ductility of the system. Niobium and vanadium have the largest impact on the ductility of the Fe–Cr–Ni system: adding 2.0 (4.0) atom % of Nb (V) raised the B/G to 2.2161 (2.2167). Cobalt reduced the B/G value and therefore decreased the ductility of the Fe–Cr–Ni system.

In Figure 6, we plot the theoretical Poisson's ratio $\nu(x)$ for paramagnetic fcc $Fe_{0.6-x}Cr_{0.2}Ni_{0.2}M_x$ (M = Al, Co, Cu, Mo, Nb, Ti, V, and W; $0 \leq x \leq 0.08$) random alloys as a function of atomic concentration x. We obtained the result that the Poisson's ratio has a similar trend to B/G. Adding Al, Cu, Mo, Nb, Ti, V, or W to the Fe–Cr–Ni alloy enhanced the value of $\nu(x)$, while Co addition decreased the $\nu(x)$ value of the Fe–Cr–Ni alloy. The most significant effects on the $\nu(x)$ value of paramagnetic fcc Fe–Cr–Ni alloy were produced by Al and V.
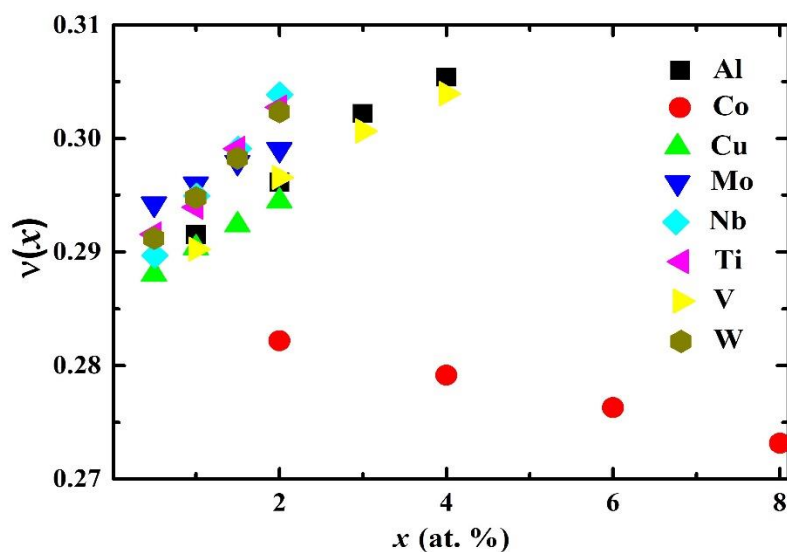

Figure 6. Theoretical Poisson's ratio $\nu(x)$ of paramagnetic fcc $Fe_{0.6-x}Cr_{0.2}Ni_{0.2}M_x$ (M = Al, Co, Cu, Mo, Nb, Ti, V, and W; $0 \leq x \leq 0.08$) quaternary alloys as a function of the atomic concentration x.

Our results on the polycrystalline elastic constants for Fe–Cr–Ni–Mo alloys are in line with those obtained by Ledbetter et al. [5], who produced ultrasonic measurements of the polycrystalline elastic constants of six fcc Fe–19Cr–12Ni (atom %) alloys with Mo content ranging up to 2.4 atom %. They found that Mo reduced the G and E moduli and raised the B and ν ratio.

4. Conclusions

Using the exact muffin-tin orbital method with coherent potential approximation and Perdew-Burke-Ernzerhof generalized gradient approximation, we investigated the single-crystal

and polycrystalline elastic parameters of paramagnetic fcc $Fe_{0.6-x}$–Cr–Ni–M_x(M = Al, Co, Cu, Mo, Nb, Ti, V, and W; $0 \leq x \leq 0.08$) random alloys. We demonstrated that all alloying elements enhanced the elastic constant C_{12} of the Fe–Cr–Ni system. Cobalt and tungsten increased the C_{11} elastic constant of the Fe–Cr–Ni ternary alloy, while other alloying elements had a negligible effect. Furthermore, we found that the C', C_{44}, E, and G moduli of the Fe–Cr–Ni alloy were increased by Co addition and reduced by Al, Cu, Mo, Nb, Ti, V, and W dopants. Tungsten had a negligible effect on C_{44}. We obtained a correlation between C' and the structural energy difference ΔE between fcc and bcc lattices, wherein large C' corresponds to large ΔE. The brittle/ductile transitions formulated by the Pugh ratio B/G were also discussed. It was shown that Al, Cu, Mo, Nb, Ti, V, and W dopants enhanced the ductility of the Fe–Cr–Ni system, while Co enhanced the brittleness of the Fe–Cr–Ni alloy. The Poisson's ratio ν showed the same trend as the B/G ratio, with small variations obtained in ν when adding alloying elements to the Fe–Cr–Ni system. Our calculations provide consistent data on the elastic properties of paramagnetic fcc Fe–Cr–Ni-based alloys at low temperature and call for experimental studies on these alloys.

References

1. Marshall, P. *Austenitic Stainless Steel: Microstructure and Mechanical Properties*; Elsevier Applied Science Publishers Ltd.: London, UK, 1984.
2. Davis, J.R. *AMS Specialty Handbook: Stainless Steels*; AMS International: Geauga County, OH, USA, 1994.
3. Wrangln, G. *An Introduction to Corrosion and Protecting of Metals*; Chapman and Hall: New York, NY, USA, 1985.
4. Majumdar, A.K.; Blanckenhagen, P.V. Magnetic phase diagram of Fe80−xNixCr20 (10≤x≤30) alloys. *Phys. Rev. B* **1984**, *29*, 4079–4085.
5. Ledbetter, H.M.; Kim, S.A. Molybdenum effect on Fe–Cr–Ni-alloy elastic constants. *J. Mater. Res.* **1988**, *3*, 40–44. [CrossRef]
6. Ledbetter, H. Predicted monocrystal elastic constants of 304-type stainless steel. *Physica* **1985**, *128*, 1–4. [CrossRef]
7. Ledbetter, H.M. Sound velocities and elastic constants of steels 304, 310, and 316. *Met. Sci.* **1980**, *14*, 595–596. [CrossRef]
8. Teklu, A.; Ledbetter, H.; Kim, S.; Boatner, L.A.; McGuire, M.; Keppens, V. Single-crystal elastic constants of Fe-15Ni-15Cr alloy. *Met. Mater. Trans. A* **2004**, *35*, 3149–3154. [CrossRef]
9. Dong, Z.; Schönecker, S.; Chen, D.; Li, W.; Long, M.; Vitos, L. Elastic properties of paramagnetic austenitic steel at finite temperature: Longitudinal spin fluctuations in multicomponent alloys. *Phys. Rev. B* **2017**, *96*, 174415. [CrossRef]
10. Vitos, L. *The EMTO Method and Applications, Computational Quantum Mechanics for Materials Engineers*; Springer: London, UK, 2007.
11. Vitos, L.; Korzhavyi, P.A.; Johansson, B. Elastic Property Maps of Austenitic Stainless Steels. *Phys. Rev. Lett.* **2002**, *88*, 155501. [CrossRef] [PubMed]
12. Hohenberg, P.; Kohn, W. Inhomogeneous Electron Gas. *Phys. Rev.* **1964**, *136*, B864. [CrossRef]
13. Kohn, W.; Sham, L.J.; Sham, L. Self-Consistent Equations Including Exchange and Correlation Effects. *Phys. Rev.* **1965**, *140*, A1133–A1138. [CrossRef]
14. Perdew, J.P.; Burke, K.; Ernzerhof, M. Generalized gradient approximation made simple. *Phys. Rev. Lett.* **1996**, *77*, 3865–3868. [CrossRef]
15. Andersen, O.K.; Jepsen, O.; Krier, G. *Lectures on Methods of Electronic Structure Calculations*; World Scientific Publishing: Singapore, 1994.

16. Andersen, O.K.; Arcangeli, C.; Tank, R.W.; Saha-Dasgupta, T.; Krier, G.; Jepsen, O.; Dasgupta, I. Third-generation TB-LMTO. *MRS Online Proc. Libr. Arch.* **1998**, *491*. [CrossRef]

17. Vitos, L.; Skriver, H.; Johansson, B.; Kollár, J. Application of the exact muffin-tin orbitals theory: The spherical cell approximation. *Comput. Mater. Sci.* **2000**, *18*, 24–38. [CrossRef]

18. Vitos, L. Total-energy method based on the exact muffin-tin orbitals theory. *Phys. Rev. B* **2001**, *64*, 014107. [CrossRef]

19. Vitos, L.; Abrikosov, I.A.; Johansson, B. Anisotropic Lattice Distortions in Random Alloys from First-Principles Theory. *Phys. Rev. Lett.* **2001**, *87*, 156401. [CrossRef] [PubMed]

20. Soven, P. Coherent-Potential Model of Substitutional Disordered Alloys. *Phys. Rev.* **1967**, *156*, 809–813. [CrossRef]

21. Györffy, B.L. Coherent-Potential Approximation for a Nonoverlapping-Muffin-Tin-Potential Model of Random Substitutional Alloys. *Phys. Rev. B* **1972**, *5*, 2382–2384. [CrossRef]

22. Kollár, J.; Vitos, L.; Skriver, H.L. *Electronic Structure and Physical Properties of Solids: The Uses of the LMTO Method*; Lecture Notes in Physics; Springer: Berlin, Germany, 2000.

23. Gyorffy, B.L.; Pindor, A.J.; Staunton, J.; Stocks, G.M.; Winter, H. A first-principles theory of ferromagnetic phase transitions in metals. *J. Phys. F Met. Phys.* **1985**, *15*, 1337–1386. [CrossRef]

24. Zhang, H.L.; Al-Zoubi, N.; Johansson, B.; Vitos, L. Alloying effects on the elastic parameters of ferromagnetic and paramagnetic Fe from first-principles theory. *J. Appl. Phys.* **2011**, *110*, 073707. [CrossRef]

25. Zhang, H.L.; Punkkinen, M.P.J.; Johansson, B.; Hertzman, S.; Vitos, L. Single-crystal elastic constants of ferromagnetic bcc Fe-based random alloys from first-principles theory. *Phys. Rev. B* **2010**, *81*, 184105. [CrossRef]

26. Delczeg-Czirjak, E.K.; Delczeg, L.; Ropo, M.; Kokko, K.; Punkkinen, M.P.J.; Johansson, B.; Vitos, L. Ab initio study of the elastic anomalies in Pd-Ag alloys. *Phys. Rev. B* **2009**, *79*, 085107. [CrossRef]

27. Al-Zoubi, N.; Johansson, B.; Nilson, G.; Vitos, L. The Bain path of paramagnetic Fe-Cr based alloys. *J. Appl. Phys.* **2011**, *110*, 013708. [CrossRef]

28. Al-Zoubi, N.; Skorodumova, N.V.; Medvedeva, A.; Andersson, J.; Nilson, G.; Johansson, B.; Vitos, L. Tetragonality of carbon-doped ferromagnetic iron alloys: A first-principles study. *Phys. Rev. B* **2012**, *85*, 014112. [CrossRef]

29. Al-Zoubi, N.; Li, X.; Schönecker, S.; Johansson, B.; Vitos, L. Influence of manganese on the bulk properties of Fe-Cr-Mn alloys: A first-principles study. *Phys. Scr.* **2014**, *89*, 125702. [CrossRef]

30. Al-Zoubi, N.; Schönecker, S.; Johansson, B.; Vitos, L. Assessing the Exact Muffin-Tin Orbitals method for the Bain path of metals. *Philos. Mag.* **2017**, *97*, 1243–1264. [CrossRef]

31. Al-Zoubi, N. First-principles study of the structural and elastic properties of Au_xV_{1-x} and Au_xNb_{1-x} alloys. *Philos. Mag.* **2018**, *98*, 1099–1113. [CrossRef]

32. Hill, R. The Elastic Behavior of a Crystalline Aggregate. *Proc. Phys. Soc. Sect. A* **1952**, *65*, 349. [CrossRef]

33. Voigt, W. Elasticitatsconstunten isotroper Korper. *Ann. Phys.* **1889**, *38*, 573. [CrossRef]

34. Reuss, A.; Angew, Z. Berechnung der Fliehgrenze von Mischkristallen auf Grund der Plastizittitsbedingung fiir Einkristalle. *Math. Phys.* **1929**, *9*, 49–58.

35. Korzhavyi, P.A.; Ruban, A.V.; Abrikosov, I.A.; Skriver, H.L.; Korzhavyi, P. Madelung energy for random metallic alloys in the coherent potential approximation. *Phys. Rev. B* **1995**, *51*, 5773–5780. [CrossRef]

36. Moruzzi, V.L.; Janak, J.F.; Schwarz, K. Calculated thermal properties of metals. *Phys. Rev. B* **1988**, *37*, 790–799. [CrossRef]

37. Dyson, D.J.; Holmes, B. Effect of alloying additions on the lattice parameter of Austenite. *J. Iron Steel Inst.* **1970**, *208*, 469–474.

38. Bain, E.C.; Dunkirk, N.Y. The nature of martensite. *Trans. Am. Inst. Min. Metall. Eng.* **1924**, *70*, 25.

39. Söderlind, P.; Eriksson, O.; Wills, J.M.; Boring, A.M. Theory of elastic constants of cubic transition metals and alloys. *Phys. Rev. B* **1993**, *48*, 5844–5851. [CrossRef] [PubMed]

40. Söderlind, P.; Wills, J.M.; Boring, A.M.; Eriksson, O. Trends of the elastic constants of cubic transition metals. *Phys. Rev. Lett.* **1992**, *68*, 2802–2805.

41. Craievich, P.J.; Sanchez, J.M.; Watson, R.E.; Weinert, M. Structural instabilities of excited phases. *Phys. Rev. B* **1997**, *55*, 787–797. [CrossRef]

42. Craievich, P.J.; Weinert, M.; Sanchez, J.M.; Watson, R.E. Local stability of nonequilibrium phases. *Phys. Rev. Lett.* **1994**, *72*, 3076–3079. [CrossRef] [PubMed]

43. Grimvall, G.; Magyari-Köpe, B.; Ozolins, V.; Persson, K.A. Lattice instabilities in metallic elements. *Rev. Mod. Phys.* **2012**, *84*, 945–986. [CrossRef]

44. Al-Zoubi, N.; Schönecker, S.; Li, X.; Li, W.; Johansson, B.; Vitos, L. Elastic properties of 4d transition metal alloys: Values and trends. *Comput. Mater. Sci.* **2019**, *159*, 273–280. [CrossRef]

45. Kollár, J.; Vitos, L.; Johansson, B.; Skriver, H. Metal Surfaces: Surface, Step and Kink Formation Energies. *Phys. Status Solidi B* **2000**, *217*, 405–418. [CrossRef]

46. Brooks, M.S.S.; Johansson, B. Exchange integral matrices and cohesive energies of transition metal atoms. *J. Phys. F Met. Phys.* **1983**, *13*, L197–L202. [CrossRef]

47. Vitos, L.; Korzhavyi, P.A.; Johansson, B. Stainless steel optimization from quantum mechanical calculations. *Nat. Mater.* **2003**, *2*, 25–28. [CrossRef] [PubMed]

48. Pugh, S.F. XCII. Relations between elastic moduli and plastic properties of polycrystalline pure metals. *Philos. Mag.* **1954**, *45*, 823–843. [CrossRef]